Parametric Decay to Lower Hybrid Waves as a Source of Modulated Langmuir Waves in Topside Ionosphere

G.V. Lizunov

Space Research Center of Polish Academy of Sciences

Y. Khotyaintsev and K. Stasiewicz

Swedish Institute of Space Physics, Uppsala Division

April 26, 2001

Short title: PARAMETRIC DECAY OF LANGMUIR WAVES

Abstract. Langmuir emissions generated by electron beams in space plasmas usually appear as chains of strongly modulated wave packets. In this article, we present a quantitative analysis of three-wave interaction between Langmuir and lower hybrid waves $L_1 \leftrightarrow L_2 + LH$, which explains many details of recent Freja observations in the topside ionosphere. The packet-like waveforms are generated as the beating of several Langmuir modes. The primary Langmuir mode (L_1) is produced by beam-plasma instability and the other modes are produced as a result of parametric decay to secondary Langmuir waves (L_2) and lower-hybrid modes (LH). We show that the decay instability has a very low threshold and high growth rate. The limited transverse dimensions of electron beams in the polar ionosphere cause radiation losses from the beam region which influence spectra of the beam-plasma and parametric instabilities.

1. Introduction

The main properties of Langmuir turbulence generated by charged particle beams in space plasma have been established during the investigation of solar radio bursts, spectra of ionospheric and magnetospheric emissions, and active space plasma experiments [*Beghin et al.*, 1989; *Shapiro and Shevchenko*, 1988; *Goldman*, 1984; *Mishin et al.*, 1989]. Recent high resolution satellite observations revealed that Langmuir emissions appear as chains of strongly modulated wave packets. The generation of modulated Langmuir emissions has been observed in auroral ionosphere [*Ergun et al.*, 1991; *Stasiewicz et al.*, 1996; *Bonnell et al.*, 1997], the solar wind [*Gurnett et al.*, 1993; *Kellogg et al.*, 1999*a*], the magnetosphere [*Kojima et al.*, 1997], as well as in laboratory plasmas [*Christiansen et al.*, 1982] and in numerical experiments in which the space plasma conditions have been simulated [*Newman et al.*, 1994; *Akimoto et al.*, 1996].

To explain these observations several hypotheses have been suggested: (i) Langmuir wave packets are solitons (or cavitons) similar to the laboratory results described by [*Nezlin*, 1981] (ii) Langmuir wave packets are spatial structures caused by the bounce-oscillations of trapped particles and propagating through the ambient plasma with wave group velocity [*Muschietti et al.*, 1995; *Akimoto et al.*, 1996] and (iii) Packet-like waveforms are the beating of two or several Langmuir waves with close frequencies. The primary wave in this case is generated due to the beam-plasma instability, the secondary harmonics appear as results of parametric decay cascade [*Ergun et al.*, 1991; *Forme*, 1993; *Hospodarsky and Gurnett*, 1995; *Robinson and Cairns*, 1995; *Stasiewicz et al.*, 1996; *Bonnell et al.*, 1997].

The first hypothesis (i) seems not to be valid in the case of ionospheric plasma because the generation of Langmuir wave packets is also observed at very low wave amplitudes where nonlinear effects are unlikely to play a role [*Stasiewicz et al.*, 1996; *Kellogg et al.*, 1999*b*]. The second explanation (ii) has been carefully examined by [*Bonnell et al.*, 1997] who showed that the wave-particle trapping process predicts modulation frequency $f_{Mod}/f_{pe} \sim 10^{-4}$, which is smaller than the modulation frequencies observed in the data set.

To focus on the third issue (iii) we show two examples from Freja data of quasi periodical modulations (Figure 1). The frequency spectra of Langmuir emissions are composed of several harmonics whose mixing produces various beating forms. The frequency difference of neighboring harmonics ($f_1 - f_2 \sim 5$ kHz) is larger than the lower-hybrid frequency of about 4 kHz which means that Langmuir waves may be parametrically connected with lower-hybrid wave. The matching conditions for three wave interactions

Figure 1

$$\omega_1 = \omega_2 + \omega_3, \tag{1}$$

$$\mathbf{k}_1 = \mathbf{k}_2 + \mathbf{k}_3$$

as analyzed by [*Stasiewicz et al.*, 1996; *Bonnell et al.*, 1997] are satisfied by a continuum of lower-hybrid modes and Langmuir modes. Since, the waveforms in Figure 1 consist of discrete harmonics, there must be a mode selection mechanism. It has been suggested by [*Stasiewicz et al.*, 1996] that the mode selection could be related to the finite size of the electron beam region which would impose the preferred $\mathbf{k}_\perp$ for lower-hybrid modes.

The goal of this work is to analyze quantitatively the process of parametric decay of a Langmuir wave generated by an electron beam to the secondary Langmuir and lower-hybrid waves, by deriving the growth rates and thresholds and taking into consideration the limited beam width and radiation losses. This article has the following composition. In section 2 we discuss the questions of the instability of superthermal electron beams registered by Freja. Further, in section 3 we advance the theory of three wave interactions $L_1 \leftrightarrow L_2 + LH$. The key role in this theory is the consideration of radiation losses from the beam region. We prove that this emission leads to the selection of separated secondary modes in the triplet of parametrically connected waves.

2. Beam-plasma instability of Langmuir waves

2.1. Freja observations

The Swedish-German satellite Freja was launched to an orbit with perigee 600 km, apogee 1750 km, and inclination 63^0 in 1992. The goal of the Freja mission was the investigation of auroral plasma processes in the topside ionosphere. A comprehensive description of the scientific payload can be found in a special issue of *Space Science Reviews (70, 405-602, 1994).* We should note here that high-frequency electric field was measured in snapshots of ~ 1 ms duration, sampled at $8 \times 10^6 s^{-1}$. The Langmuir frequency is typically less than the electron cyclotron frequency $\omega_p < \omega_c$ which introduces some peculiarities in the dispersion equation. Another important condition is that in many cases the ion temperature is higher than the electron temperature $T_i > T_e$ which leads to the strong damping of ion acoustic waves.

The bursts of Langmuir emissions had been observed simultaneously with the appearance of superthermal electron beams and therefore are associated with the beam-plasma instability. The registered distribution functions of superthermal electrons are wide in velocity space $\Delta V_b \sim V_b$ (V_b is the average beam velocity, ΔV_b is electron velocity spreading), and the reduced "one-dimensional" distribution functions are close to the plateau or weak "bump in tail" type of distribution. However, a measurement of the distribution function of superthermal electrons takes about 65 ms, a time too long to adequately observe the expected evolution of the distribution function. In Figure 3 we show examples of the electron beam observed in association with the emission in Figure 1a. In Table 1 we show the values of plasma and beam parameters observed on Freja. The bottom row contains parameters relevant for this event.

Figure 3

Table 1

2.2. Generation of primary Langmuir waves

The theoretical analysis reveals certain disagreement between calculated and observed spectra of Langmuir waves. Let's examine this problem.

According to Freja observations electron beams are weak ($n_b \ll n_p$) and have spread velocity spectrum ($\Delta V_b \sim V_b$). In this case the instability growth rate is [*Shapiro and Shevchenko*, 1988]:

$$\gamma_b \sim \left(\frac{V_b}{\Delta V_b}\right)^2 \frac{n_b}{n_p}\omega, \tag{2}$$

where $\omega = \omega(\mathbf{k})$ is the frequency of the Langmuir wave. The dispersion relation of the Langmuir wave is [*Pelletier et al.*, 1988]

$$\omega = \omega_p[1 + 3(k\lambda_D)^2 - A\sin^2\theta]^{1/2}, \tag{3}$$

where $A = 1/(1 - \omega_p^2/\omega_c^2)$, λ_D is Debye radii and θ is the direction of wave propagation in respect to the magnetic field. Waves generated at larger angles from the magnetic field should significantly depart from the Langmuir frequency which contradicts observations that emission spectra consist of several narrow lines (Figure 1). An outstanding question is what determines the observed narrowness of the Langmuir wave spectrum. A similar question appeared in the article of [*Newman et al.*, 1994]. The authors explained the spectrum narrowing by the Doppler damping of oblique Langmuir waves. The calculations were done for the specific set of ionospheric plasma parameters $\omega_p \approx \omega_c$ when the Doppler shifted wave velocity

$$V_{DR} = \frac{\omega - \omega_c}{k} \approx \frac{\omega_p - \omega_c}{\omega_p} V_b \tag{4}$$

falls into thermal electron speed and resonates with bulk electrons. In our case $\omega_c > \omega_p$, and the velocity (4) is out of the region of plasma distribution function.

We shall investigate further the hypothesis that the damping of oblique Langmuir waves may be explained by the influence of transverse limitation of the beam width [*Jones and Kellogg*, 1973]. The electron beams which generate Langmuir waves appear to be related to Alfvénic structures which have a transverse size of 50-500 m, comparable to the inertial electron length $\lambda_e = c/\omega_p$ at Freja altitudes [*Stasiewicz et al.*, 1997; *Bellan and Stasiewicz*, 1998]. Effective damping caused by Langmuir wave emission from the beam region can be estimated as

$$\nu_{eff} \sim |V_{g\perp}| / R_b = (AV_b/R_b)\theta, \tag{5}$$

where R_b is the beam width and the group velocity $V_{g\perp}$ implied by (3) is

$$V_{g\perp} = \partial\omega/\partial k_\perp = k^{-1}\partial\omega/\partial\theta \approx -AV_b\theta. \tag{6}$$

Here $k_\perp$ is the perpendicular to the magnetic field component of the wave vector, and we study the case when $\theta \ll 1$, $\sin\theta \to \theta$. The wave damping limits the sphere of instability by the condition $\gamma_b \geq \nu_{eff}$ or

$$\theta \leq \theta_{\max} = \frac{\gamma_b R_b}{A V_b}. \tag{7}$$

For the parameters indicated in the Table 1 and $R_b = 300\ m$, $V_b = 3 \times 10^8$ cm/s, $A \approx 1$, we find that $\gamma_b = 10^3\ s^{-1}$, $\theta_{\max} \approx 0.1\ rd$, and $\Delta\omega \sim 0.01\omega_p$ which corresponds well with the observed width of Langmuir wave spectrum. Table 1

3. Parametric decay $L_1 \to L_2 + LH$

3.1. Experimental background

Short duration of the HF snapshots (1 ms) and frequency response of the filter in HF channel make it impossible to analyze waves in a range from 1 to 10 kHz on the basis of HF channel only. Spectrum taken from both HF and MF (sampled at $32 \times 10^3 s^{-1}$) clearly shows enhanced wave power near LH frequency (1-10 kHz) together with strong peak at plasma frequency (see Figures 2 and 4 in [*Stasiewicz et al.*, 1996]). Due to the design of the F4 instrument on Freja both channels cannot be sampled simultaneously and therefore a time lag exists between two measurements, making direct comparison of HF and MF waveforms difficult. However, it is possible to make a statistical comparison of wave activity around LH frequency and modulation frequency of Langmuir waves, under the assumption that Langmuir and LH activity usually observed in localized region related to large-scale Alfvénic turbulence. We present a comparison of two such measurements in Figure 3. Figure 3 Solid line represents a region of enhanced wave activity around LH frequency measured in MF channel and asterisk shows the location of modulation frequency observed in HF channel. In 70% of cases modulation frequency is within the range of LH waves. The rest of the data may be explained by the assumption that HF and MF measurements are made in different regions due to high spacecraft velocity (7 km/s) and fine localization of Langmuir activity.

3.2. Dispersion properties

The equations for the non-linear wave-wave interaction for the Langmuir waves as well as for the lower-hybrid waves have been written in the literature in quite general form [*Sturman*, 1976; *Ergun et al.*, 1991; *Kellogg et al.*, 1992; *Sharma et al.*, 1992]. In this section we present the analysis relevant to the Freja experimental conditions. Let us consider the case where the primary wave is generated by the beam and secondary harmonics appear as a result of parametric decay (or decay cascade) of the primary wave to Langmuir and low-frequency plasma wave, namely, the lower-hybrid mode as indicated by Freja observations [*Stasiewicz et al.*, 1996; *Bonnell et al.*, 1997]. We should mention that there are other competing parametric processes. One of them is the usual parallel decay channel into a field-aligned Langmuir wave and an ion-acoustic wave, which may be negligible for the relatively low electron temperature $T_i > T_e$ assumed here. The other possibility is the parametric decay into a short oblique-Langmuir wave and a short oblique-ion wave [*Akimoto*, 1995]. Relative effectiveness of this mechanism will be estimated below.

The primary Langmuir wave L_1 propagates along the magnetic field because the growth rate of beam-plasma instability reaches the maximum value at $\theta = 0$. The oblique Langmuir wave L_2 and lower-hybrid wave LH are generated as results of parametric decay (see Figure 4). In the Freja environment $k\lambda_D = V_{Te}/V_b \sim 0.1$ which allows us to neglect the term $3(k\lambda_D)^2 \ll 1$ in the dispersion equation (3). For $\theta = 0$ we get for the primary mode: Figure 4

$$\omega_1 = \omega_p, \quad k_{x1} = 0, \quad k_{z1} = k_0 = \omega_p/V_b. \tag{8}$$

The secondary Langmuir wave is slightly oblique with $\theta \sim 0.1$ rd for the characteristic frequency shift of secondary wave $\omega_1 - \omega_2 \sim 0.01\omega_p$. In this case term $A\sin^2\theta \approx A\theta^2 \ll 1$ and the dispersion relation (3) is simplified considerably and given for the secondary wave

$$\omega_2 = \omega_p \left(1 - A\theta^2/2\right), \quad k_{x2} = k_\perp = k_0\theta, \quad k_{z2} \approx k_0. \tag{9}$$

The dispersion relation for the lower-hybrid waves was given by [*Shapiro et al.*, 1993]; see also Appendix A):

$$\omega_3 = \omega_{lh}\left[1 + \frac{M}{m}\cos^2\theta_3 + \frac{1}{2}(k_3\lambda_T)^2 - \frac{\alpha}{(1+\alpha)}(k_3\lambda_e)^{-2}\right]^{1/2}, \tag{10}$$

where $\alpha = \omega_p^2/\omega_c^2$, $\omega_{lh} = \omega_{pi}/\sqrt{1+\alpha}$ is lower-hybrid frequency, ω_{pi} is ion Langmuir frequency, m is electron mass, M is ion mass, θ_3 is the direction of lower-hybrid wave propagation ($\theta_3 \approx \pi/2$), $\lambda_T^2 = 3T_i/(\omega_{lh}^2 M) + 2\alpha T_e/[\omega_c^2 m(1+\alpha)]$ is a spatial scale comparable with Debye radii, and $\lambda_e = c/\omega_p$ is the electron inertial length. As we can see in Figure 3, the wave vector of lower-hybrid wave is $k_3 \sim k_\perp \ll k_0$, which is why the relation $k_3^2\lambda_T^2 \ll 1$ is fulfilled. We can also neglect $(k_3\lambda_e)^{-2} \ll 1$. As a result we obtain for the lower-hybrid mode

$$\omega_3 = \omega_{lh}\sqrt{1+(M/m)\cos^2\theta_3}, \quad k_{x3} = -k_\perp, \quad k_{z3} = k_\perp \cos\theta_3. \tag{11}$$

Connecting quantities (11) with wave numbers and frequencies (8), (9) by matching conditions (1) we obtain also:

$$\omega_3 = A\omega_p \frac{\theta^2}{2}, \quad k_{x3} = -k_0\theta, \quad k_{z3} = Ak_0\frac{\theta^3}{2}g(\theta), \tag{12}$$

where the function $g(\theta)$ is:

$$g(\theta) = \left[(1+\alpha)(1-\theta_{\min}^4/\theta^4)\right]^{1/2}, \tag{13}$$

and $\theta_{\min}^4 = (4m/M)(1-\alpha)^2/(1+\alpha)$. The relations (8), (9), (12) determine wave vectors and frequencies of interacting waves through the single free parameter θ. From (13) we can see that θ is limited from the below: $\theta \geq \theta_{\min}$. We can easily understand the origin of this cutoff by taking into account the fact that the difference frequency of parametrically connected Langmuir waves cannot be smaller than the lower-hybrid frequency $\omega_3 = \omega_1 - \omega_2 \geq \omega_{lh}$. The case $\theta = \theta_{\min}$ corresponds to the generation of lower-hybrid oscillations with $k_{z3} = 0,\ \omega_3 = \omega_{lh}$. For $\alpha = \omega_p^2/\omega_c^2 = 0.25$ and effective ion mass $M = 4M_p$ (calculated for the 80% [O^+] and 20% [H^+] ion composition) the cutoff angle is $\theta_{\min} = 0.13$ rd.

3.3. Equations for three-wave interaction

The thermal and electromagnetic corrections to the plasma waves dispersion laws are small because $(k_3\lambda_T)^2 \ll (k_{1,2}\lambda_D)^2 \ll 1$, $(k_3\lambda_e)^2 \gg 1$. This means that the Langmuir and lower-hybrid waves may be considered in this case as quasi-potential modes of cold magnetized plasma. This makes it possible to simplify calculations further by solving the problem in hydrodynamic approximation with $\mathbf{E} = -\nabla\varphi$. The evolution of waves is described in terms of slowly varying amplitude:

$$\varphi_\alpha(t, \mathbf{r}) = \Phi_\alpha(t, \mathbf{r}) \exp\{i(\omega_\alpha t - \mathbf{k}_\alpha \cdot \mathbf{r})\}, \tag{14}$$

where index $\alpha = 1, 2$ refers to the Langmuir waves, $\alpha = 3$ refers to the lower-hybrid wave. The nonlinear equation for wave amplitude is [*Kadomtsev*, 1988]:

$$\omega_\alpha \frac{\partial \varepsilon_{eff}}{\partial \omega} \left(\frac{\partial}{\partial t} + \mathbf{V}_{gr}^\alpha \cdot \nabla \right) \Phi_\alpha(t, \mathbf{r}) = \frac{4\pi}{k_\alpha^2} \left(\mathbf{k}_\alpha \cdot \mathbf{j}_\alpha \right) \exp\{-i(\omega_\alpha t - \mathbf{k}_\alpha \cdot \mathbf{r})\}, \tag{15}$$

where ε_{eff} is the effective dielectric permeability of cold magnetized plasma (see Appendix A), $\mathbf{V}_{gr}^\alpha$ is the group velocity of plasma wave, $\mathbf{j}_\alpha$ is the nonlinear current synchronized with wave 'α'. This current is generated by two other waves accordingly to

$$\begin{aligned}
\mathbf{j}_1 &= -e(\delta n_{e2}\mathbf{V}_{e3} + \delta n_{e3}\mathbf{V}_{e2}) + e(\delta n_{i2}\mathbf{V}_{i3} + \delta n_{i3}\mathbf{V}_{i2}) \\
\mathbf{j}_2 &= -e(\delta n_{e1}\mathbf{V}^*_{e3} + \delta n^*_{e3}\mathbf{V}_{e1}) + e(\delta n_{i1}\mathbf{V}^*_{i3} + \delta n^*_{i3}\mathbf{V}_{i1}), \qquad (16) \\
\mathbf{j}_3 &= -e(\delta n_{e1}\mathbf{V}^*_{e2} + \delta n^*_{e2}\mathbf{V}_{e1}) + e(\delta n_{i1}\mathbf{V}^*_{i2} + \delta n^*_{i2}\mathbf{V}_{i1}).
\end{aligned}$$

The calculation of nonlinear currents (16) is presented in Appendix B. Using the expressions for $\mathbf{j}_\alpha$ and $\omega_\alpha \partial\varepsilon_{eff}/\partial\omega$ obtained in the Appendix we finally get:

$$\begin{aligned}
\left(\frac{\partial}{\partial t} + \mathbf{V}_{gr1}\cdot\nabla\right)\Phi_1 &= -i\beta_1\Phi_2\Phi_3, \\
\left(\frac{\partial}{\partial t} + \mathbf{V}_{gr2}\cdot\nabla\right)\Phi_2 &= -i\beta_1\Phi_1\Phi_3^*, \qquad (17) \\
\left(\frac{\partial}{\partial t} + \mathbf{V}_{gr3}\cdot\nabla\right)\Phi_3 &= -i\beta_3\Phi_1\Phi_2^*,
\end{aligned}$$

where $\beta_1 = (e/2mV_b)k_0\theta g(\theta)$, $\quad \beta_3 = (e/2mV_b)k_0[\alpha + \theta g(\theta)]/(1-\alpha^2)$.

3.4. The effect of radiation losses

According to the Freja data the electron beams are usually associated with Alfvénic structures [*Stasiewicz et al.*, 1996; *Khotyaintsev et al.*, 2000] which have transverse dimensions of $R_b \sim 50 \div 500m$. Estimating the rate of radiation losses caused by the wave emission from the beam region as $\mathbf{V}_{gr}\cdot\nabla \sim V_{g\perp}/R_b = \nu_\alpha$, we can write (17) as:

$$\frac{\partial}{\partial t}\Phi_1 \quad = \quad -i\beta_1\Phi_2\Phi_3,$$

$$\frac{\partial}{\partial t}\Phi_2 = -i\beta_1\Phi_1\Phi_3^* - \nu_2\Phi_2, \tag{18}$$
$$\frac{\partial}{\partial t}\Phi_3 = -i\beta_3\Phi_1\Phi_2^* - \nu_3\Phi_3,$$

where $\nu_2 = |V_{g\perp 2}|/R_b = AV_b\theta/R_b$, $\nu_3 = |V_{g\perp 3}|/R_b = g(\theta)\nu_2/(2(1+\alpha))$. Here we take into account that the transverse component of group velocity of primary Langmuir wave is equal to zero, so that $\nu_1 = 0$; ν_2 is determined by expression (5) and the group velocity of the lower-hybrid wave is calculated from (11) as $V_{g\perp 3} = -AV_b\theta g(\theta)/[2(1+\alpha)]$. Assuming that $\Phi_1 = \Phi_0 = const$, $\Phi_{2,3} \propto \exp\{\gamma t\}$, we find the instability growth rate:

$$\gamma = -\frac{\nu_2+\nu_3}{2} + \sqrt{\Gamma^2 + (\nu_2-\nu_3)^2)/2}, \tag{19}$$

where $\Gamma = (e/2mV_b)(E_0/\sqrt{1-\alpha^2})\sqrt{\theta g(\theta)\,(\alpha+\theta g(\theta))}$ is the value of growth rate in the absence of dissipation, $E_0 = k_0\Phi_0$ is the amplitude of primary wave electric field. The instability exists if $\gamma > 0$. Substituting to (19) expressions for Γ, ν_2, ν_3, we get the explicit dependence of the growth rate on axial angle θ:

$$\gamma' = \frac{\gamma}{\Gamma_0} = -\left(1+\frac{g(\theta)}{2(1+\alpha)}\right)p\theta + \left[\theta g(\theta)\,(\alpha+\theta g(\theta)) + \left(1-\frac{g(\theta)}{2(1+\alpha)}\right)^2 p^2\theta^2\right]^{1/2}, \tag{20}$$

where $\Gamma_0 = eE_0/\left[2mV_b\sqrt{1-\alpha^2}\right]$ is the pumping parameter, $p = V_b/[2R_b(1-\alpha)\Gamma_0]$ is a dimensionless parameter of dissipation. As it follows from (20) the condition of instability $\gamma > 0$ realizes when

$$\theta_{\min} < \theta < \theta_{\max} = \frac{\alpha(1+\alpha)}{2p^2-(1+\alpha)}, \tag{21}$$

where $\theta_{\rm min}$ has been determined in (13). For $p > \sqrt{(1+\alpha)/2}$ or

$$\frac{V_b}{R_b} > \frac{eE_0}{mV_b\sqrt{2(1-\alpha)}}, \tag{22}$$

the instability exists in a limited range of θ-angles. The growth rate of instability $\gamma(\theta)$ reaches the maximum at the angle $\theta_0 \leq \theta_{\rm max}$, where $\theta_{\rm max}$ is given by expression (21). In the case of opposite inequality $p \leq \sqrt{(1+\alpha)/2}$ we have no restriction on axial angle, the instability has a wide-band character, and the growth rate (20) increases monotonically with θ. Figure 5 demonstrates the dependence (20) $\gamma = \gamma(\theta)$ for various p. Figure 5

For the parameters indicated in Table 1, $R_b = 300\ m$, $E_0 = 200$ mV/m we find: $p \approx 1$ (curve "b" on Figure 4), $\theta_0 = 0.2$ rd, $\gamma = 2.5 \times 10^2\ s^{-1}$. The frequency shift between the primary and the secondary Langmuir modes (12) in this case is $\omega_3 = \omega_1 - \omega_2 = 0.02\omega_p$ which has very good correspondence with experimental data. Figure 6 represents the waveform $E(t) = E_1(t) + E_2(t)$ obtained by solving equations (18) for the angle θ_0 and numerical parameters indicated here. One can notice details which correspond to the three characteristic time scales of the problem: the high frequency filling of wave packets with frequency $\omega = (\omega_1 + \omega_2)/2 \approx \omega_p$, beating with the difference frequency $\omega_3 = \omega_1 - \omega_2$, and the slow modulation of beating with frequency $\sim \Gamma$. Saturation of the decay instability is caused mainly by the energy transfer from the primary to secondary waves and during the time interval $\sim \Gamma^{-1}$ wave attenuation is small. We would like to emphasize good Figure 6 correspondence of the calculated function $E(t)$ with observed waveforms (as for example in Figure 1 and many others published in the literature).

In this work we haven't examined the possibility of pump wave cascading into the numerous oblique Langmuir waves. But one may note that the effectiveness of the cascading process is restricted by the radiation damping (5) that rises for next harmonics $\sim \theta$.

Decay instability $L_1 -> L_2 + LH$ operates similarly to the parametric instability $L -> oL + oI$ that has been investigated by [*Akimoto*, 1995] earlier (here oL denotes a short oblique Langmuir wave and oI denotes a short oblique ion wave). The instabilities growth rates are correlated with each other as $(\gamma/\Gamma)^2 \sim \sqrt{T_e/(T_e+T_i)}\sqrt{m/M}(4k_0\lambda_D)^{-1}$, where γ is given by expression (3) in the paper of [*Akimoto*, 1995], Γ is determined above in expression (19), $k_0 = \omega_p/V_b$ is pumping wave vector. For the parameters assumed here parametric decay $L_1 -> L_2 + LH$ is more efficient: $\gamma/\Gamma \sim 0.1$.

4. Conclusion

The generation of Langmuir wave packets is a common phenomenon registered in laboratory and space conditions with a great diversity of plasma parameters. In this article we present the theory of the parametric generation of Langmuir wave packets on the basis of Freja observations for the conditions in upper auroral ionosphere summarized in Table I: $\omega_p < \omega_c$, $T_e \leq T_i$. In such conditions the beam driven Langmuir wave decays to a secondary Langmuir and a lower-hybrid wave $L_1 \to L_2 + LH$. The decay instability has a very low threshold and high growth rate (20). The peculiarity of the considered parametric process is related to the fact that under condition $\omega_p < \omega_c$ both lower-hybrid and Langmuir modes belong to the same dispersion branch of plasma waves: $\omega_{lh} < \omega < \omega_p$. Langmuir oscillations $\omega = \omega_p$ in this case are not separated from oscillations with lower frequencies which is why three wave decay can take place in a wide range of the difference frequencies $\omega_3 = \omega_1 - \omega_2$.

In our article we show for the first time that the transverse limitation of electron beams propagating in the auroral ionosphere causes the selection of separated secondary harmonics from continuous spectra of Langmuir and lower-hybrid waves. As it follows from (5) wave emissions from the beam region add to the system effective (radiation) dissipation, in this case $\nu_{eff} \propto \theta$. The dependence of decay instability growth rate (20) $\Gamma(\theta)$ is more complicated. When $\theta < \alpha$ the growth rate is $\Gamma \propto \sqrt{\theta}$, which is why the instability is always "stronger" than the dissipation in a region of small θ-angle. When θ is larger the decay instability has threshold (22). When the instability is suppressed (condition (22) is satisfied) the Langmuir wave is generated in narrow zone $\theta_{\min} < \theta < \theta_{\max}$, closely to $\theta_0 \sim 0.2$ rd. In this case the envelope of the Langmuir wave is periodically modulated with the difference frequency $\omega_3 \sim 0.02\omega_p$. Figure 6 represents the waveform calculated for this case. If condition (22) is not satisfied, the parametric instability generates the wide spectrum of oblique Langmuir waves whose mixing produces irregularly modulated waveforms. Both types of modulated Langmuir waves have been observed by Freja.

Appendix A: Effective dielectric permeability

As it follows from dispersion relations (3) and (10) it is a good approximation to consider Langmuir and lower-hybrid waves as quasi-potential modes of cold magnetized plasma. These modes are derived from the hydrodynamic dispersion equation [*Kadomtsev*, 1988]

$$\varepsilon_{eff} = \left(1 - \frac{\omega_{pe}^2}{\omega^2 - \omega_{ce}^2} - \frac{\omega_{pi}^2}{\omega^2 - \omega_{ci}^2}\right)\sin^2\theta + \left(1 - \frac{\omega_{pe}^2}{\omega^2}\right)\cos^2\theta = 0, \qquad \text{(A1)}$$

where ε_{eff} is an effective dielectric permeability. Langmuir waves appear as solution of (A1) at $\theta \to 0$, $\omega \sim \omega_p$:

$$\varepsilon_{eff} \approx 1 - \frac{\omega_{pe}^2}{\omega^2} - \frac{\omega_{ce}^2}{\omega_{pe}^2 - \omega_{ce}^2}\sin^2\theta = 0. \qquad \text{(A2)}$$

In this case

$$\omega\frac{\partial\varepsilon_{eff}}{\partial\omega} = 2\frac{\omega_{pe}^2}{\omega^2} \approx 2,\ \ \omega = \omega_p\sqrt{1 - A\sin^2\theta}, \qquad \text{(A3)}$$

where $A = (1 - \omega_{pe}^2/\omega_{ce}^2)^{-1}$. The lower-hybrid mode is the solution of (A1) at $\theta \to \pi/2\,\omega \sim \omega_{lh} \gg \omega_{ci}$. In this case:

$$\varepsilon_{eff} \approx \left(1 + \frac{\omega_{pe}^2}{\omega_{ce}^2} - \frac{\omega_{pi}^2}{\omega^2}\right)\sin^2\theta - \frac{\omega_{pe}^2}{\omega^2}\cos^2\theta = 0, \qquad \text{(A4)}$$

The dispersion relation (11) (without thermal and EM corrections) immediately follows from this equation. Let's write also the expression for the derivative:

$$\omega\frac{\partial\varepsilon_{eff}}{\partial\omega} = 2\left(1+\frac{\omega_{pe}^2}{\omega_{ce}^2}\right). \tag{A5}$$

We emphasize that under condition $\omega_{pe} < \omega_{ce}$, the lower-hybrid and Langmuir modes are the opposite edges of a single dispersion branch of plasma waves: $\omega_{lh} < \omega < \omega_p$.

Appendix B: Nonlinear currents calculation

Nonlinear currents $\mathbf{j}_\alpha$ are determined by equations (16). Our goal is to express the variations of density and velocity $\delta n_\alpha, \mathbf{V}_\alpha$ through the potentials $\varphi_\alpha(t,\mathbf{r}) = \Phi_\alpha(t,\mathbf{r})\exp\{i(\omega_\alpha t - \mathbf{k}_\alpha\cdot\mathbf{r})\}$. The set of initial equations consists of the linearized hydrodynamic equations of movement and continuity:

$$\begin{aligned}\frac{\partial}{\partial t}\mathbf{V}_\alpha^e &= \frac{e}{m}\nabla\varphi_\alpha - \mathbf{V}_\alpha^e\times\omega_{ce} \\ \frac{\partial}{\partial t}\delta n_\alpha^e &= -n_p\nabla\cdot\mathbf{V}_\alpha^e,\end{aligned} \tag{B1}$$

with solutions

$$\begin{aligned}V_{\alpha x}^e &= -\frac{e}{\omega_\alpha m}\frac{k_{\alpha x}}{1-\omega_c^2/\omega_\alpha^2}\varphi_\alpha, \\ V_{\alpha z}^e &= -\frac{e}{\omega_\alpha m}k_{\alpha z}\varphi_\alpha, \\ \delta n_\alpha^e &= -\frac{en_p}{m\omega_\alpha^2}\left(\frac{k_{\alpha x}^2}{1-\omega_{ce}^2/\omega_\alpha^2}+k_{\alpha z}^2\right)\varphi_\alpha,\end{aligned} \tag{B2}$$

(for the electronic component). The solution for the ion variations V_α^i, δn_α^i, we obtain from (B1) by the replacement of $m\to M$, $e\to -e$, $\omega_{ce}\to\omega_{ci} = (m/M)\omega_{ce}$.

Substituting to (B1) expressions (8), (9), (12) for the frequencies and wave numbers ω_α, $\mathbf{k}_\alpha$, we find the quantities $\delta n_\alpha, \mathbf{V}_\alpha$ in each wave. For the primary Langmuir wave L_1:

$$
\begin{aligned}
V^e_{x1} &= 0, \\
V^e_{z1} &= -\frac{e}{mV_b}\varphi_1, \quad V^i_{z1} \ll V^e_{z1}, \\
\delta n^e_1 &= -\frac{en_p}{mV_b^2}\varphi_1, \quad \delta n^i_1 \ll \delta n^e_1.
\end{aligned}
\tag{B3}
$$

For the secondary wave L_2:

$$
\begin{aligned}
V^e_{x2} &= \frac{e}{mV_b}A\frac{\omega_{pe}^2}{\omega_{ce}^2}\theta\varphi_2, \quad V^i_{x2} \ll V^e_{x2}, \\
V^e_{z2} &= -\frac{e}{mV_b}\varphi_2, \quad V^i_{z2} \ll V^e_{z2}, \\
\delta n^e_2 &= -\frac{en_p}{mV_b^2}\varphi_2, \quad \delta n^i_2 \ll \delta n^e_2.
\end{aligned}
\tag{B4}
$$

For the lower-hybrid wave LH:

$$
\begin{aligned}
V^e_{x3} &= -\frac{e}{mV_b}\frac{\omega_3\omega_{pe}}{\omega_{ce}^2}\theta\varphi_3, \quad V^i_{x3} = -\frac{e}{MV_b}\frac{\omega_{pe}}{\omega_3}\theta\varphi_3, \\
V^e_{z3} &= -\frac{e}{mV_b}\theta g(\theta)\varphi_3, \quad V^i_{z3} \ll V^e_{z3}, \\
\delta n^e_3 &= -\frac{en_p}{mV_b^2}\theta^2\left(g^2(\theta) - \frac{\omega_{pe}^2}{\omega_{ce}^2}\right)\varphi_3, \quad \delta n^i_3 = \frac{en_p}{mV_b^2}\theta^2\frac{\omega_{pi}^2}{\omega_3^2}\varphi_3.
\end{aligned}
\tag{B5}
$$

Placing (B2)-(B4) into equations (16), we find the dependence of nonlinear currents on wave potentials. The simplification of further calculations is possible because we can neglect the majority of terms in (16). We use the fact that parameter θ is small: $\theta \ll 1$. In the primary Langmuir wave the variations $\delta n_1, \mathbf{V}_1$ do not depend from θ: $\delta n_1, V^e_{z1} = O(1)$. In the secondary wave: $\delta n_2, V^e_{z2} = O(1)$, $V^e_{x2} = O(\theta)$. In the lower-hybrid wave: $V^e_{x3}, V^i_{x3}, V^e_{z3} = O(\theta)$, $\delta n^e_3, \delta n^i_3 = O(\theta^2)$. Keeping in equations (17) terms of the lowest order in θ and neglecting ion terms in comparison with corresponding electron terms, we get after some transformations:

$$
\begin{aligned}
\mathbf{k}_1 \cdot \mathbf{j}_1 \quad &\approx -k_0(e\delta n^e_2 V^{e*}_{z3}) = -\tfrac{e}{4\pi m V_b} k_0^3 \theta g(\theta) \varphi_2 \varphi_3^*, \\
\mathbf{k}_2 \cdot \mathbf{j}_2 \quad &\approx -k_0(e\delta n^e_1 V^{e*}_{z3}) = -\tfrac{e}{4\pi m V_b} k_0^3 \theta g(\theta) \varphi_1 \varphi_3^*, \\
\mathbf{k}_3 \cdot \mathbf{j}_3 \quad &\approx -k_{x3}(e\delta n^e_1 V^{e*}_{x2}) - k_{z3} e \left(\delta n^e_1 V^{e*}_{z2} + \delta n^{e*}_2 V^e_{z1}\right) \\
&\approx -\tfrac{e}{4\pi m V_b} k_0^3 A \theta^2 \left[\tfrac{\omega_{pe}^2}{\omega_{ce}^2} + \theta g(\theta)\right] \varphi_1 \varphi_2^*,
\end{aligned}
\tag{B6}
$$

where $k_0 = \omega_{pe}/V_b$.

Acknowledgments. G.V. Lizunov would like to acknowledge support from Svenska Institutet (Visby program) during his stay in IRF-Uppsala.

References

Akimoto, K., Parametric instabilities of Langmuir waves in strong magnetic fields and phase transition of langmuir turbulence, *Phys. Plasmas*, *2*, 649, 1995.

Akimoto, K., Y. Omura, and H. Matsumoto, Rapid generation of Langmuir wave packets during electron beam-plasma instabilities, *Phys. Plasmas*, *3*, 2559–2563, 1996.

Beghin, C., J. L. Rauch, and J. M. Bosqued, Electrostatic plasma waves and auroral hiss generated at low altitude, *J. Geophys. Res.*, *94*, 1359–1378, 1989.

Bellan, P., and K. Stasiewicz, Fine-scale cavitation of ionospheric plasma caused by inertial Alfvén wave ponderomotive force, *Phys. Rev. Lett.*, *80*, 3523–3526, 1998.

Bonnell, J., P. Kintner, J.-E. Wahlund, and J. Holtet, Modulated Langmuir waves: Observations from Freja and SCIFER, *J. Geophys. Res.*, *102*, 17,233–17,240, 1997.

Christiansen, P., V. Jain, and J. Bond, Laboratory beam-plasma interaction - linear and nonlinear, in *Artificial particle beams in space plasma studies*, edited by B. Grandal, pp. 439–470, Plenum Press, 1982.

Ergun, R. E., C. W. Carlson, J. P. McFadden, J. H. Clemmons, and M. H. Boehm, Evidence of a transverse Langmuir modulational instability in space plasma, *Geophys. Res. Lett.*, *18*, 1177, 1991.

Forme, F., A new interpretation of the origin of enhanced ion acoustic fluctuations in the upper ionosphere, *Geophys. Res. Lett.*, *20*, 2347–2350, 1993.

Goldman, M. V., Strong turbulence of plasma waves, *Rev. Mod. Phys.*, *56*, 709–735, 1984.

Gurnett, D. A., G. B. Hospodarsky, W. S. Kurth, D. J. Williams, and S. J. Bolton, The fine structure of Langmuir waves produced by a solar electron event, *J. Geophys. Res.*, *98*, 5631–5637, 1993.

Hospodarsky, G. B., and D. A. Gurnett, Beat-type Langmuir wave emissions associated with a type ii solar radio bursts: evidence of parametric decay, *Geophys. Res. Lett.*, *22*, 1161, 1995.

Jones, T., and P. Kellogg, Plasma waves artificially induced in the ionosphere, *JGR*, *78*, 2166, 1973.

Kadomtsev, B., *Collective phenomena in plasma (in Russian)*, Moscow: Nauka, 1988.

Kellogg, P., K. Goetz, N. Lin, S. Monson, A. Balogh, R. Forsyth, and R. Stone, Low frequency magnetic signals associated with Langmuir waves, *GRL*, *19*, 1299, 1992.

Kellogg, P., K. Goetz, S. Monson, and S. Bale, Langmuir waves in a fluctuating solar wind, *JGR*, *104*, 17069, 1999*a*.

Kellogg, P., K. Goetz, S. Monson, and S. Bale, Langmuir waves in a fluctuating solar wind, *JGR*, *104*, 6751, 1999*b*.

Khotyaintsev, Y., N. Ivchenko, K. Stasiewicz, and M. Berthomier, Electron energization by Alfvén waves: Freja and sounding rocket observations, *Physica Scripta*, *T84*, 151, 2000.

Kojima, H., H. Furuya, H. Usui, and H. Matsumoto, Modulated electron plasma waves observed in the tail lobe: Geotail waveform observations, *Geophys. Res. Lett.*, *24*, 3049, 1997.

Mishin, E., Y. Ruzin, and V. Telegin, *Interaction of electron beams with ionospheric plasma (in russian)*, Moscow: Gidrometeoizdat, 1989.

Muschietti, L., I. Roth, and R. Ergun, Kinetic localization of beam-driven Langmuir waves, *J. Geophys. Res.*, *100*, 17,481–17,490, 1995.

Newman, D. L., M. V. Goldman, R. E. Ergun, and M. H. Bohem, Langmuir turbulence in the auroral ionosphere: 1. linear theory, *J. Geophys. Res.*, *99*, 6367–6376, 1994.

Nezlin, V., Observation of Langmuir solitons, in *Plasma Physics, Advances in science and technology in the USSR*, edited by B. Kadomtsev, pp. 144–175, MIR Publishers, Moscow, 1981.

Pelletier, G., H. Sol, and E. Asseo, Magnetized Langmuir wave packets excited by a strong beam-plasma interaction, *Phys. Rev. A.*, *38*, 2552–2563, 1988.

Robinson, P. A., and I. H. Cairns, Maximum Langmuir fields in planetary foreshocks determined from the electrostatic decay threshold, *GRL*, *22*, 2657, 1995.

Shapiro, V. D., and V. I. Shevchenko, Astrophysical plasma turbulence 1, *Astrophys. Space Sci. Rev.*, *6*, 427, 1988.

Shapiro, V. D., V. I. Shevchenko, G. I. Solovev, V. P. Kalinin, R. Bingham, R. Z. Sagdeev, M. Ashour-Abdalla, J. Dawson, and J. J. Su, Wave collapse at the lower-hybrid resonance, *Phys. Fluids B*, *5*, 3148–3162, 1993.

Sharma, R., Y. Tripathi, A. AlJanabi, and R. Boswell, Parametric excitation of electrostatic whistler waves by electron plasma waves, *JGR*, *97*, 4275, 1992.

Stasiewicz, K., B. Holback, V. Krasnoselskikh, M. Boehm, and P. Kinter, Parametric instabilities of Langmuir waves observed by Freja, *J. Geophys. Res.*, *101*, 21,515–21,525, 1996.

Stasiewicz, K., G. Gustafsson, G. Marklund, P.-A. Lindqvist, J. Clemmons, and L. Zanetti, Cavity resonators and Alfvén resonance cones observed on Freja, *J. Geophys. Res.*, *102*, 2565–2575, 1997.

Sturman, B., Plasma turbulence near the lower-hybrid resonance, *Soviet Phys. JETP*, *71*, 613, 1976.

G.V. Lizunov, Space Research Center PAS, Bartycka 18A, 00716, Warsaw, Poland. Permanent address: Astronomy and Space Physics Dept., Kyiv Shevchenko University, Glushkov pr. 6, 252023, Ukraine (e-mail: liz@galaxy.ups.kiev.ua)

Y. Khotyaintsev, K. Stasiewicz, Swedish Institute of Space Physics, Box 537, S-751 21 Uppsala, Sweden (e-mail: yuri@irfu.se, ks@irfu.se)

Received ____________________

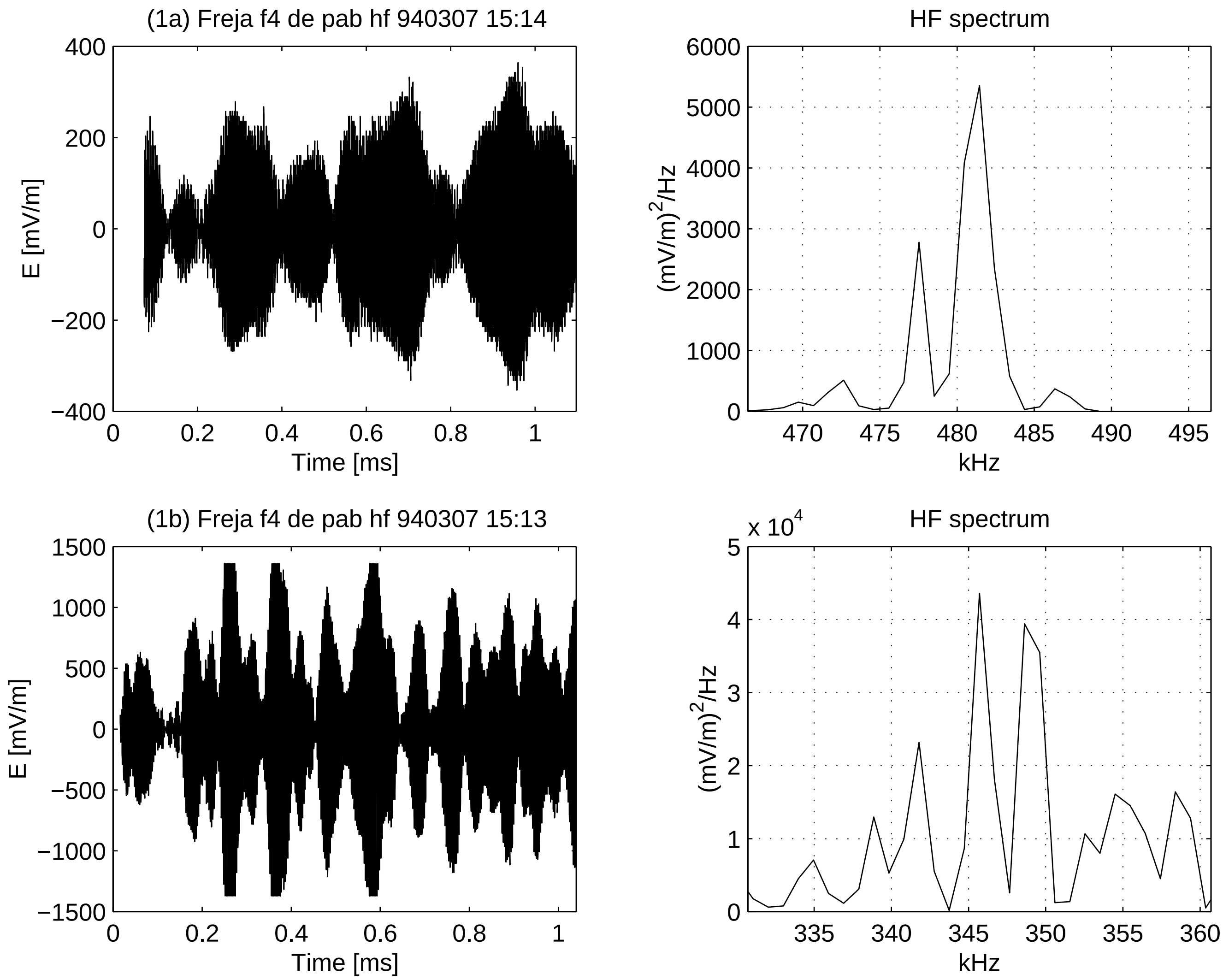

Figure 1. Two examples of waveforms (left) and spectral composition (right) of Langmuir emissions registered by Freja on March 7, 1994 at 1513 UT.

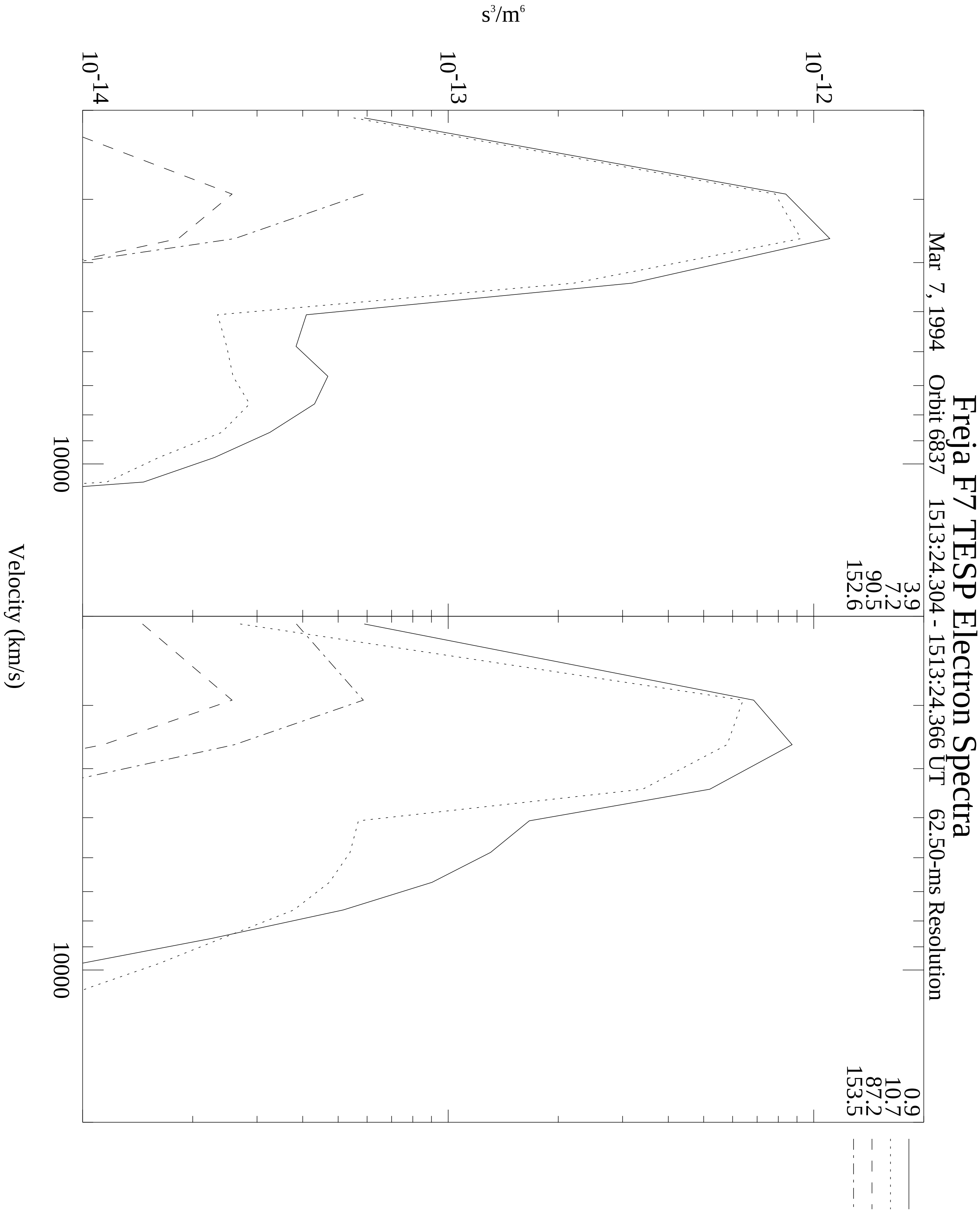

Freja F7 TESP Electron Spectra
Mar 7, 1994 Orbit 6837 1513:24.304 - 1513:24.366 UT 62.50-ms Resolution
s³/m⁶
10-12
10-13
10-14
10000
10000
Velocity (km/s)
3.9
7.2
90.5
152.6
0.9
10.7
87.2
153.5

Figure 2. The velocity distribution function of superthermal electrons for various pitch-angles.

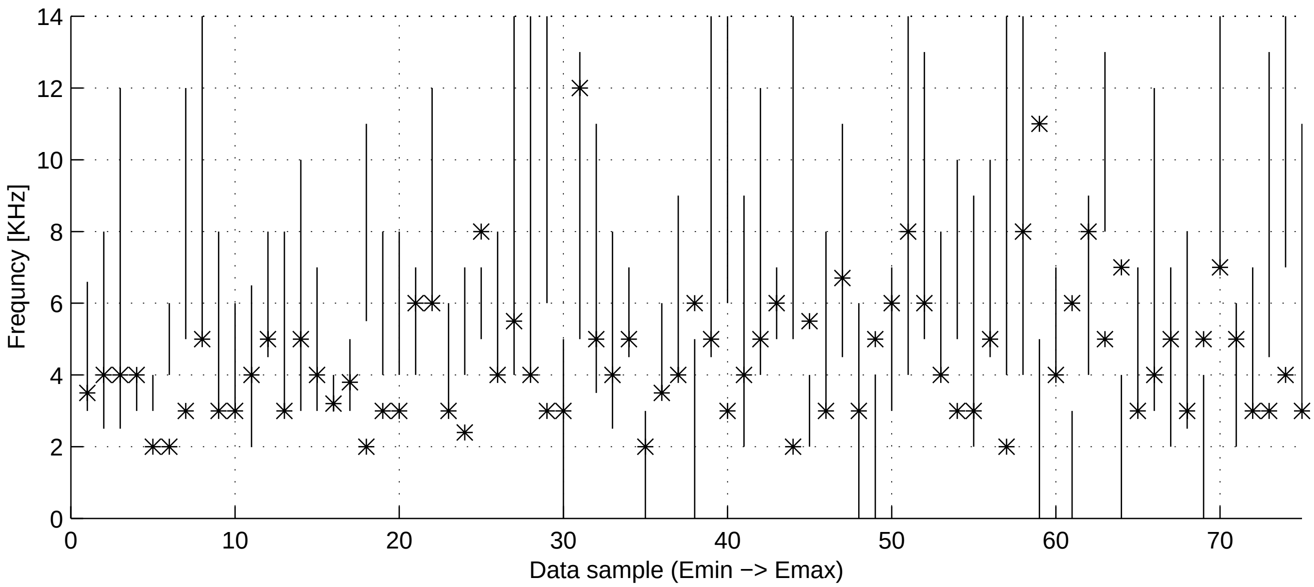

Figure 3. LH frequency range (solid line) and modulation frequency (*) for two neighbor snapshots in MF and HF channels.

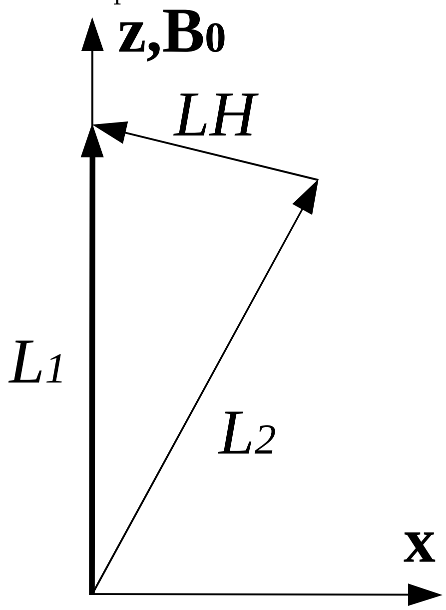

Figure 4. Illustration of the k-vectors in the problem of three-wave interaction. $L_{1,2}$ are the wave vectors of primary and secondary Langmuir waves, LH is the vector of lower-hybrid wave.

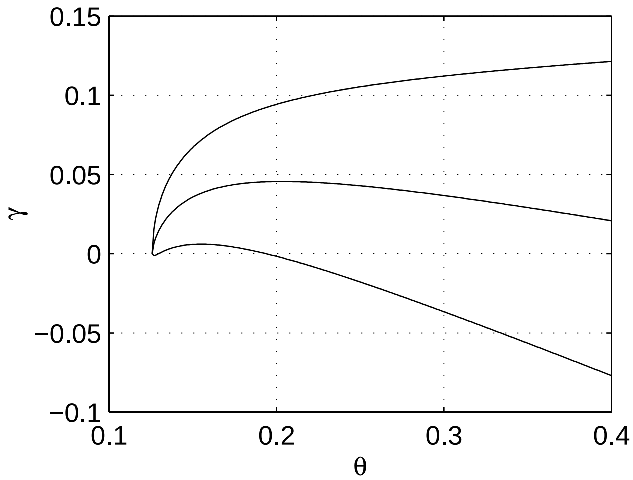

Figure 5. Normalized growth rate of decay instability (equation (20)) for various parameters n: a) $n = 0.8$, b) $n = 1$, c) $n = 1.2$ and $\alpha = 0.25$.

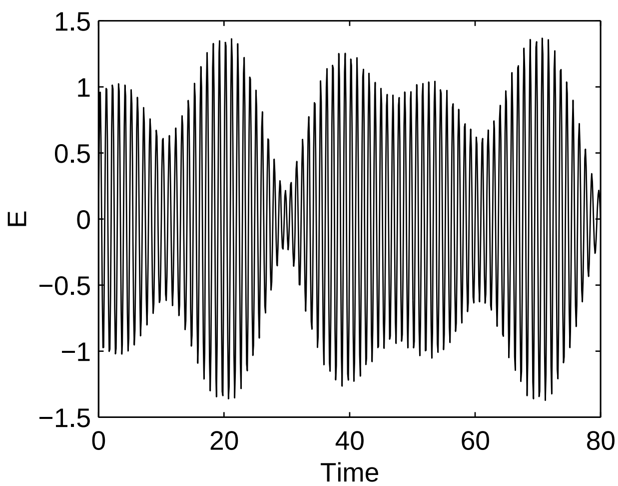

Figure 6. Theoretically calculated waveform for parameters indicated in the text.

$n_p,\ cm^{-3}$	$\omega_p,\ s^{-1}$	$\omega_c,\ s^{-1}$	$V_{Te},\ cm/s$	$n_b,\ cm^{-3}$	$E_b,\ eV$	$V_b,\ cm/s$	$\Delta V_b,\ cm/s$
$400 \div 3600$	$(1 \div 4) \times 10^6$	5×10^6	4×10^7	$0.1 \div 1$	$10 \div 1500$	–	–
1200	2×10^6	5×10^6	4×10^7	1	$10 \div 100$	3×10^8	2×10^8

Table 1. Plasma parameters of topside polar ionosphere according to Freja observations. On the bottom row there are values of parameters registered at 94.03.07 1513 UT (orbit 6837). Here E_b, V_b, ΔV_b are the energy, average velocity and velocity spread of superthermal electrons respectively.